

Access to this work was provided by the University of Maryland, Baltimore County (UMBC) ScholarWorks@UMBC digital repository on the Maryland Shared Open Access (MD-SOAR) platform.

Please provide feedback

Please support the ScholarWorks@UMBC repository by emailing [scholarworks-group@umbc.edu](mailto:scholarworks-group@umbc.edu) and telling us what having access to this work means to you and why it's important to you. Thank you.



# A Magnetic Pressure Front Upstream of the Heliopause and the Heliosheath Magnetic Fields and Plasma, Observed during 2017

L. F. Burlaga<sup>1</sup> , N. F. Ness<sup>2</sup>, D. B. Berdichevsky<sup>3,4</sup>, L. K. Jian<sup>5</sup> , J. Park<sup>2,5</sup> , P. Mostafavi<sup>6,7</sup> , and J. D. Richardson<sup>8</sup>

<sup>1</sup> MC 673, NASA/GSFC, Greenbelt, MD 20771, USA

<sup>2</sup> University of Maryland, UMBC, MD, USA

<sup>3</sup> MC 672, NASA/GSFC, Greenbelt, MD 20771, USA

<sup>4</sup> IFIR/UNR-CONICET, Esmeralda y 27 de Febrero, 2000 Rosario, Sta Fe, Argentina

<sup>5</sup> Heliophysics Science Division, NASA Goddard Space Flight Center, Greenbelt, MD 20771, USA

<sup>6</sup> Department of Space Science, University of Alabama in Huntsville, Huntsville, AL 35899, USA

<sup>7</sup> Department of Astrophysical Sciences, Princeton University, Princeton, NJ 08544, USA

<sup>8</sup> Kavli Center for Astrophysics and Space Research, Massachusetts Institute of Technology, Cambridge, MA, USA

Received 2019 January 21; revised 2019 April 2; accepted 2019 April 5; published 2019 May 21

## Abstract

*Voyager 1* (V1), moving in the interstellar magnetic field, observed an increase in the daily averages of  $B$  beginning on day  $\approx 346$ , 2016, rising to a local maximum on day  $\approx 382$ , and declining nearly monotonically for the most part until day 720, measured from 2016.0. A pressure front was observed during a  $\approx 35$ -day interval beginning on day 346, 2016. The pressure front observed by V1 was not a shock, although one might expect it to evolve into a shock. *Voyager 2* (V2) observed the distant heliosheath during 2017. The average  $B$  in the heliosheath was relatively high, 0.130 nT. The distribution of azimuthal angles had two nearly equal maxima at approximately  $90^\circ$  and  $180^\circ$ . An unusual transition of the  $BT$  component from a large “away” sector to a large “toward” sector occurred during 2017 from day 101 to day 239. Abrupt but small changes in magnetic polarity occurred between day 146 and day 239, when the average  $BT$  component of  $B$  was close to zero. Changes in the  $>70$  MeV nucleon<sup>-1</sup> cosmic-ray intensity were qualitatively related to the  $B(t)$  profile described by the CR- $B$  relationship. There was no net decrease in magnetic flux at V2 in the heliosheath during 2017 that might be attributed to ongoing magnetic reconnection in the heliosheath. Small-scale increments in  $B$  can be described by a  $q$ -Gaussian distribution with  $q = 1.64 \pm 0.02$  for hourly averages of  $B$  and  $q = 1.54 \pm 0.08$  for daily averages of  $B$ .

**Key words:** ISM: magnetic fields – Sun: heliosphere – Sun: magnetic fields

## 1. Introduction

*Voyager 1* (V1) crossed the termination shock and entered the heliosheath on approximately 2004 day 350 (Burlaga et al. 2008; Decker et al. 2008; Gurnett & Kurth 2008; Richardson et al. 2008; Stone et al. 2008). At that time, the position of V1 was (94.0 au,  $34.7^\circ$  latitude and  $253.0^\circ$  longitude) in solar ecliptic coordinates. Later, *Voyager 1* crossed a new boundary region in which three abrupt increases in  $B$  and two abrupt decreases in  $B$  were observed from 2012 days 210 to 236, at which time the position of V1 was near  $35.0^\circ$  latitude and  $121.5^\circ$  (Burlaga et al. 2013, 2014; Krimigis et al. 2013; Stone et al. 2013). This region was not unambiguously identified as the heliopause at that time. The region was associated with interstellar magnetic fields that entered the heliosheath as a result of an instability (Krimigis et al. 2013). Burlaga et al. (2013) suggested that the fifth increase in  $B$  on  $\approx 2012/238$  corresponds to the final crossing of the heliopause and entry into the “draped interstellar magnetic fields” (Whang 2010), which have been observed by V1 up to the present time (2019 March 19). Although Fisk & Gloeckler (2014) and Gloeckler & Fisk (2016) argue that V1 is still in the heliosheath, it is now generally recognized that V1 is moving through the interstellar magnetic field, since Gurnett et al. (2013) determined that the density beyond that boundary was  $0.06 \text{ cm}^{-3}$ , consistent with the density of interstellar plasma. Gurnett et al. (2018) have detected seven electron plasma oscillation events in the very local interstellar medium (VLISM), including two recent events that occurred from days 213 to 249 in 2017, and from days 150 to 157 in 2018. They found that the density increased with

distance during this interval, consistent with the “density ramp” describing the increase in density with distance beyond the heliopause that was identified by Gurnett et al. (1993). Pogorelov et al. (2017) describe the region observed by Gurnett et al. (2018) as a “boundary layer” or “a density depletion region.”

Pogorelov et al. (2017) used the term “bow wave” to describe the larger region, extending a few hundred au upstream of the heliopause, that is significantly influenced by the motion of the Sun. Holzer (1989) introduced the term “VLISM” to describe the region within 0.01 pc,  $\sim 2000$  au, of the Sun. Zank (2015) redefined the VLISM as the region of the ISM surrounding the Sun that is modified by the deposition of heliospheric material or, equivalently, the region in the LISM (within at least 75 au of the heliopause) in which neither proton nor electron collisions can equilibrate the pickup ions with the thermal plasma. Zank’s definition of the VLISM describes the region that the *Voyager 1* is observing beyond the heliopause.

*Voyager 1* (V1), moving in the VLISM, observed a large magnetic feature characterized by an increase in the daily averages of  $B$  beginning on 2016 day 346, rising to a local maximum on day 382, and declining nearly monotonically for the most part until day 720, measured from 2016.0. During the year 2017, V1 moved from 137.15 to 140.72 au in the VLISM, and its latitude and longitude changed from  $35.0^\circ$  to  $35.1^\circ$  and from  $255.8^\circ$  to  $250.0^\circ$ , respectively. A pressure front was observed during a  $\approx 35$ -day interval in which  $B$  increased, beginning on 2016 day 346. Unlike the 2012 shock wave, which was a collisional shock with a thickness of  $\sim 5$  days (Mostafavi & Zank 2018a, 2018b), the 2017 pressure front with

the thickness of  $\sim 35$  days cannot be a shock. Nevertheless, the pressure front might evolve into a collisional shock, whose characteristics are determined by heat conduction (Baranov & Ruderman 2013) and possibly other factors.

Let us now introduce the discussion of recent *Voyager 2* (V2) observations in the heliosheath. *Voyager 2* crossed the termination shock on approximately 2007/244 (Burlaga et al. 2008; Decker et al. 2008; Gurnett & Kurth 2008; Richardson et al. 2008; Stone et al. 2008), when it was at 83.7 au,  $-31.6^\circ$  latitude, and  $288.8^\circ$  longitude. During the year 2017, which will be discussed in this paper, V2 moved through the heliosheath from 113.15 to 116.31 au, its latitude increased from  $-35.1^\circ$  to  $-36.2^\circ$ , and its longitude changed from  $290.1^\circ$  to  $290.2^\circ$ . The angle between V1, the Sun, and V2 was  $73^\circ$ . The distance that V2 moved from the time it crossed the termination shock to the end of 2017 is 27.5 au, which is larger than the distance 23.5 au that V1 moved between the termination shock and heliopause. One should note that the radial extent of the termination shock changes with time by a small amount (10 au) and the radial extent of the heliopause changes even less ( $\sim 3$ –4 au).

The observations of the magnetic fields and plasma by V2 in the heliosheath are strongly related to the sunspot cycle, which is associated with variations in the solar activity. Although V1 was moving through the draped interstellar magnetic fields, the V1 observations during 2016 and 2017 were also influenced by motions of the heliopause and by disturbances in the heliosheath and solar wind. Thus, both the V1 observations upstream of the heliopause and V2 observations in the heliosheath during 2017 were related to the solar activity during the declining phase of sunspot cycle 24, which began in 2009 January (see Jian et al. 2011); <http://www.sidc.be/silso/monthlyssnplot> and <http://www.sidc.be/silso/>. An extensive set of references to the observations made up to the maximum of the sunspot cycle 24 is in Burlaga et al. (2018).

## 2. Observations of a Magnetic Feature and Pressure Front by VOYAGER 1 in the VLISM during 2016–2017

Figure 1 shows that the magnetic field observed by V1 from 2016 day 1 to day 700 (measured from the beginning of 2016) reveals the existence of a distinct large-scale magnetic feature in the VLISM characterized by a relatively abrupt increase in  $B$  during an interval of  $\sim 35$  days from 2016 day 346 to day 381, followed by a more or less linear decay until at least day 700. Since we lack plasma observations of the speed, density, and temperature of the feature, we cannot determine the flow structure and its associated dynamics of this large magnetic field structure. The average magnetic field strength during 2016 and 2017 was  $0.43 \pm 0.02$  nT (Figure 1(a)). The average azimuthal angle ( $\lambda$ ) during this 2 yr interval (Figure 1(b)) was  $\langle \lambda \rangle = 282^\circ \pm 4^\circ$ , and the average elevation angle (Figure 1(c)) was  $\langle \delta \rangle = 25^\circ \pm 2^\circ$ .

The origin of the large-scale magnetic feature beginning at the end of 2016 and extending through 2017 is probably related to a disturbance in the heliosphere and heliosheath and the accompanying motion of the heliopause. Zirnstien et al. (2018) and McComas et al. (2018) observed a “pressure front” (a relatively fast increase in the solar wind ram pressure followed by an extended region of high pressure) that passed 1 au in 2014 and reached as far as the *IBEX* ribbon. This pressure front might have evolved into a shock in the VLISM. Other efforts have been made to identify and model the evolution of systems of flows near the Sun that produce the shocks and radio wave

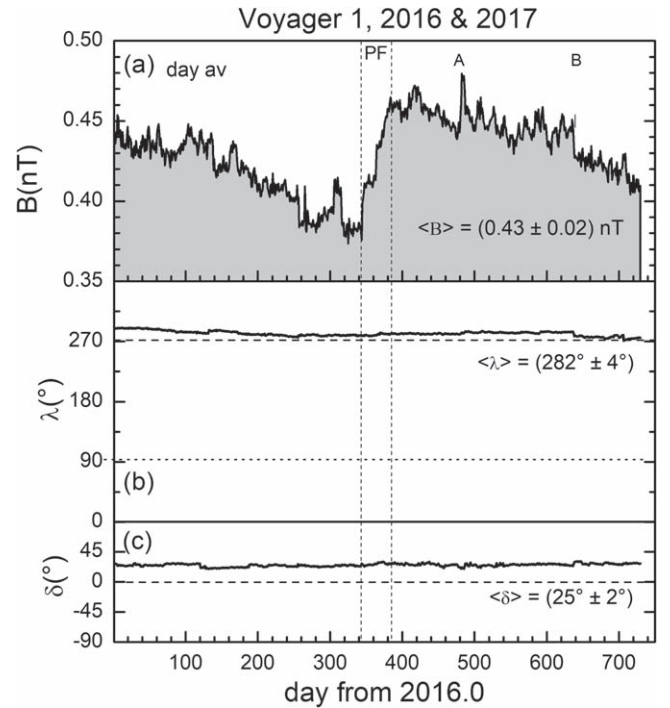


**Figure 1.** *Voyager 1* observed a large magnetic structure characterized by an increase in the yearly averages of  $B$  beginning on 2016 day 346, rising to a local maximum on day 381, and declining nearly monotonically until day 720, measured from 2016.0. The vertical dashed lines in panel (a) show a  $\sim 35$ -day interval in which the magnetic field and hence the magnetic pressure were increasing. We call this region a “pressure front,” labeled “PF” in the figure. The direction of  $B$  was nearly constant from day 1 (2016.0) to day 730, with average azimuthal angle  $\lambda = 282^\circ \pm 4^\circ$  and average elevation angle  $\delta = 25^\circ \pm 2^\circ$ .

bursts observed at V1 in the VLISM. It will be of interest to look for systems of transient flows in the solar wind that might produce a magnetic field structure like that in Figure 1. Fermo et al. (2015), Zirnstien et al. (2018), and McComas et al. (2018) show how a pressure front can evolve through the heliosphere, termination shock, and heliosheath and modify the structure of the *IBEX* ribbon.

We shall now discuss in detail the abrupt increase in  $B$  observed by V1, beginning on 2016 day 346, which we refer to as a “magnetic pressure front,” or simply “pressure front,” since the increase in  $B$  corresponds to an increase in magnetic pressure.

A high-resolution plot of the 48 s averages of  $B$  in the interval from day 270 to day 480, measured from 2016.0, is shown in Figure 2. This interval shows the detailed structure of the pressure front. Note that there are two kinds of noise in this figure: Gaussian noise indicated by the width of the band of points, and nearly discontinuous jumps that are related to systematic errors. *Voyager 1* observed that  $B$  increased by  $B2/B1 = 1.19 \sim 20\%$ , as shown in Figure 2. The jumps in  $B$  at the vertical dashed lines in Figure 2 occurred in less than 10 minutes. These jumps cannot be shocks, since the shock observed by V1 in the VLISM during 2012 (which accelerated energetic electrons) moved past the spacecraft in approximately 5 days (Burlaga et al. 2013), whereas the pressure front moved past the spacecraft in 35 days.

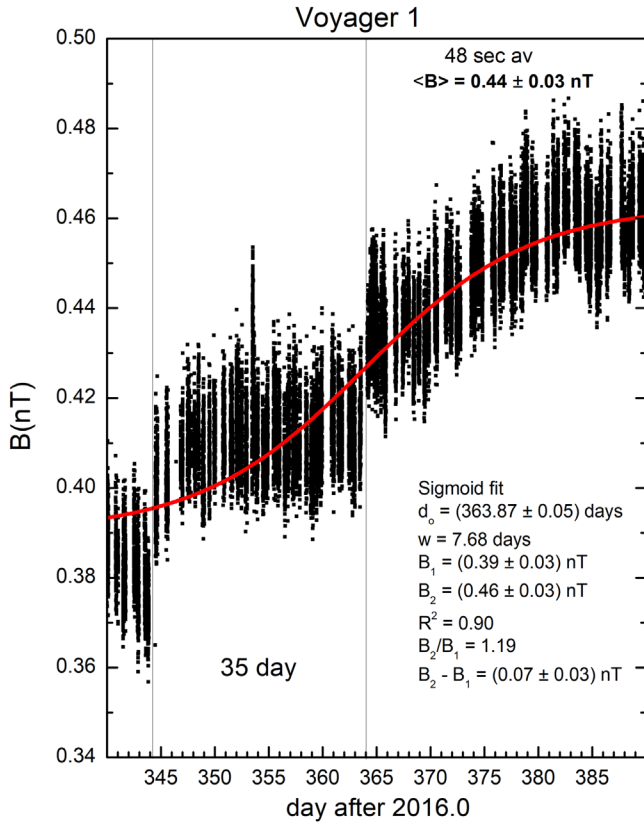


**Figure 2.** Plot of 48 s averages of the magnetic field strength by *Voyager 1* from day 340 to day 380, measured from 2016.0, showing the pressure front (PF) and the regions before and after it. The pressure front is described by a sigmoid fit to the observations, which gives a smooth curve describing the pressure front, that passes through essentially all of the data points. Two types of noise are evident in this figure: Gaussian noise, and nearly discontinuous systematic jumps in  $B$ . The jumps in  $B$  at the beginning and in the middle of the pressure wave occur within a few minutes, so they did not correspond to shocks, which would have moved past the spacecraft in only  $\approx 5$  days.

The magnetic field strength profile of the pressure front observed by *VI* (Figure 2) can be fit with the sigmoid function

$$B(t) = B_2 + \{B_1 - B_2\} / \{1 + \exp(t - t_0)/\tau\}. \quad (1)$$

A smooth fit to these data was obtained using the sigmoid distribution, with the coefficient of determination  $R^2 = 0.90$ . The curve describing the increase in the magnetic field strength across the pressure front is shown by the red curve in Figure 2. This smooth curve passes through all of the measurements within the limits of the fluctuations of the measurements. The uncertainty in the  $BT$  and  $BN$  components is approximately 0.03 nT, and the uncertainty in the  $BR$  component could be 2 times as large, but the  $BR$  component is very small. Thus, the uncertainty in  $B$  is approximately  $\pm 0.035$  nT. The magnetic field strength increased across the pressure front by a factor of  $B_2/B_1 = 1.19$ , from  $B_1 = 0.39 \pm 0.03$  nT to  $B_2 = 0.46 \pm 0.03$  nT. The passage time (“width”) of the 2016/2017 pressure front was estimated to be  $\sim 35$  days as indicated by the two vertical dashed lines in Figure 2. The Boltzmann fit gives a width parameter  $w = 7.6$  days, so 80% of the passage time is  $\tau = 4.4 \times w$  (Burlaga et al. 2011), which gives  $\tau = 33.4$  (days), in good agreement with the number of  $\approx 35$  days obtained by visual inspection of the data. The inflection point of the Boltzmann fit is at day 363.87, which is midway

between the two vertical dashed lines, corresponding to the pressure front.

The increase  $B$  across the pressure front shown in Figure 2 is a real physical feature, but it is far too extended to be a shock wave, since the passage time was  $\tau \approx 33.4$  days, which is large compared to the time of the shock passage observed by *VI* during 2012, which was  $\tau \approx 5$  days. On the other hand, the magnetic pressure does increase across the interval, and such an increase in  $B$  and the corresponding pressure should propagate. There might be a corresponding increase in density, which would indicate a compression wave, but the density cannot be measured by *VI*. The pressure front is expected to steepen as it moves away from the heliopause, and at some distance it should steepen into a shock. In the interstellar plasma, the collisional mean free path decreases with increasing distance from the heliopause, because the density increases with distance in the “boundary layer” or “density ramp” as discussed above. Therefore, the shock should form closer to the heliopause than it would in the absence of the boundary layer.

It should be relatively easy to model the evolution of a magnetic pressure front like that shown in Figure 2, by studying the motions of a spherical global merged interaction region (GMIR) as it approaches the heliopause, interacts with it, and produces a pressure front propagating in the VLISM. By definition, a GMIR moves past a spacecraft during one or more solar rotations, which is consistent with the pressure front discussed above that moved past *Voyager 1* in  $\approx 35$  days. The plasma and magnetic field parameters in the GMIRs observed in the distant heliosheath by *V2* during 2012 (Burlaga & Ness 2016) and 2015 (Burlaga et al. 2018) could be used as inputs to the model.

There appear to be a series of quasi-periodic oscillations in  $B(t)$  during the interval A–B within the large magnetic feature shown in Figure 1. These oscillations are shown in more detail in Figure 3, where they occur between  $\sim 2017/114$  and  $2017/272$ . The amplitudes of the fluctuations are close to the statistical uncertainty  $\pm 0.03$  nT of the  $BR$  and  $BT$  components of  $B$ , so that one must be cautious in interpreting them. Nevertheless, (1) the relatively abrupt but small increase in  $B$  at the beginning of the interval, (2) the decrease in  $B$  from 0.44 to 0.43 nT in less than 15 hr at the end of the interval (day 272.42), and (3) the quasi-periodic oscillations of the fluctuations within this interval suggest that they could be physically significant and that they are worthy of further study using data from the other instruments on *V2*.

### 3. Relationship between the Magnetic Fields Observed in the Heliosheath and Magnetic Fields Observed in the VLISM

Ideally, one would like to have continuous observations of the magnetic fields for two extended intervals on a radial line from the Sun, with one point in the heliosheath and the other in the VLISM. Unfortunately, such observations do not exist. Thus, in order to predict or determine the cause of observations of magnetic fields in the VLISM, it is necessary to use some suitable initial conditions based on observations in the heliosphere and/or heliosheath together with theoretical models. In this paper, we simply compare observations made in the VLISM and in the heliosheath during 2017 in order to demonstrate the great contrast in the observations between these two regions.



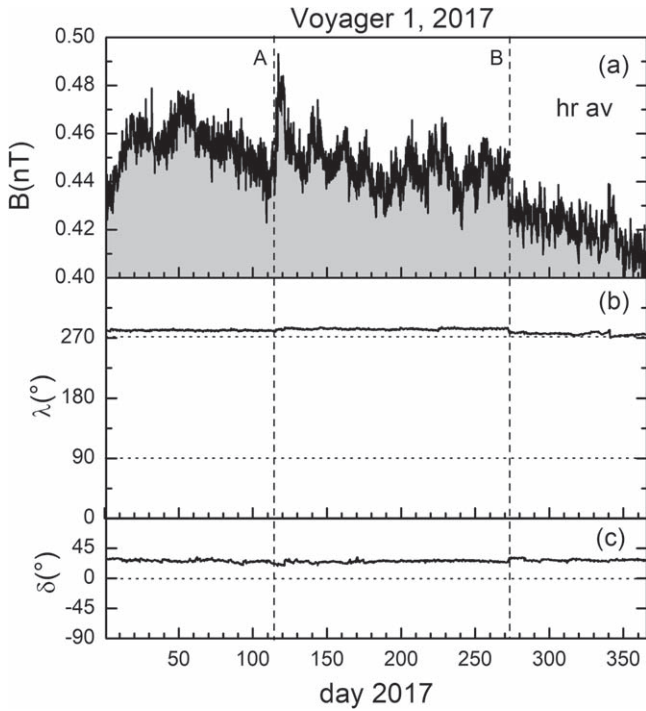


**Figure 3.** Unusual sequence of quasi-periodic oscillations in  $B$  observed during an interval in the declining portion of the structure shown in Figure 1. This interval began with a relatively large increase in  $B$  ( $\approx 0.04$  nT) at  $\approx 2017$  day 114 (marked by A in Figure 1), and it ended abruptly within 15 hr on 2017 day 272.4 when  $B$  decreased abruptly by 0.017 nT (marked B in Figure 1).

It is instructive to digress briefly in order to reference some published results that have been obtained concerning the relationship between the VLISM and heliosphere/heliosheath. We emphasize that there are features and processes occurring in the draped interstellar magnetic field and relatively near the heliopause that are causally related to the structures and processes occurring in the heliosheath that are amenable to observational and theoretical studies.

Gurnett et al. (1993) presented remote observations made by the plasma wave system (PWS instrument) on *Voyager 1*, which they interpreted as a result of an interplanetary shock that propagated across the heliopause into the LISM. Whang & Burlaga (1995) published a 1D spherically symmetric MHD model with pickup protons that describes the process discussed by Gurnett et al. (1993) as a shock wave in the VLISM driven by a GMIR. They found that when a GMIR shock interacts with the heliopause, it produces a reflected shock that moves back through the heliosheath and a shock that moves outward into the bow wave. A recent model by Fermo et al. (2015) follows the evolution of an MIR as it moves past the termination shock, through the heliosheath, and generates a pressure wave in the VLISM. Washimi et al. (2011, 2017) used a 3D time-dependent MHD/gasdynamic model to calculate the interaction of a high ram pressure front or shock with the heliopause, resulting in the reflection of the pressure front toward the termination shock and a propagating pulse beyond the heliopause.

Observational evidence for the existence of shock waves beyond the heliopause and in the VLISM was found by the PWS instrument and magnetometer (MAG) on *VI*. Two abrupt “jumps” in ISMF strength, near day 336, 2012.92 and 236, 2014.65, were observed. Both of these disturbances were preceded by electron plasma oscillation events that are

indicators of shocks (Gurnett et al. 2015). Other plasma and radio waves were observed by the PWS instrument that were not accompanied by increases in  $B$  and abrupt changes in the magnetic field such as the pressure pulse discussed in Section 2 that were observed by MAG but not by the PWS instrument.

A number of models attempted to describe the evolution of the solar wind from 1 au, through the heliosheath, and beyond (Zank et al. 1996; Baranov & Zaitsev 1998; Zank & Müller 2003; Liu et al. 2007, 2014; Pogorelov et al. 2012a, 2013; Opher et al. 2011; Borovikov et al. 2012; Opher 2012; Provornikova et al. 2013, 2014; Fermo et al. 2015; Michael et al. 2015; Zirnstein et al. 2016).

A comprehensive model of magnetic fields, particles, shocks, and pressure waves in the solar wind, the heliosheath, and the region beyond the heliopause (Kim et al. 2017) used a 3D five-fluid model (Borovikov et al. 2012; Pogorelov et al. 2014), with observations of the plasma and magnetic field at 1 au as initial conditions to simulate observations of the magnetic field and plasma in the VLISM. They predicted four major increases in  $B$  and density between 2013 and 2020. The first event arrived at *VI* near 2012.92, which corresponds to the shock discussed by Burlaga & Ness (2016). This shock was found to be unexpectedly broad, with a thickness of about 8.7 days (Burlaga et al. 2013), and the “jump” in  $B$  is often referred to as “shock-like.” However, Mostafavi & Zank (2018a, 2018b) showed that it could be a collisional shock, whose thickness is determined by the collisional mean free path rather than the ion inertial length or cyclotron radius. The second event arrived at *VI* near 2014.65, which is comparable to the arrival time of the shock, 2014.648, inferred from the plasma wave and magnetic field observations (Gurnett et al. 2015).

The third event was predicted by the model of Kim et al. (2017) to arrive at *VI* near 2017.395. It might be related to the GMIR observed by *V2* during 2015 described by Burlaga et al. (2018), but this relationship will be discussed in a separate study. Richardson et al. (2017), predicted that a shock would be observed by *VI* in early 2018, based on plasma observations from *V2* of an extended region with high densities and temperatures. We shall soon have observations that will determine whether or not such a shock did arrive at *VI*. Kim et al. (2017) predicted that a fourth shock will be observed by *VI* on 2019.502.

## 4. Observations of the Heliosheath Magnetic Field during 2017 by *VOYAGER 2*

### 4.1. Daily Average Magnetic Fields and Sectors

We now turn from the observations made by *VI* beyond the heliosheath in the VLISM during 2017 to the observations made by *V2* in the distant heliosheath. During 2017, *V2* was observing magnetic fields and the flows from the Sun during the declining phase of solar cycle 24.

Near the beginning of sunspot cycle 24, during 2010, *V2* was sampling the solar wind and magnetic fields that left the Sun near solar minimum during 2009. The heliospheric current sheet (HCS) was near the solar equatorial plane. The polarity of the magnetic field in the southern hemisphere at *V2* was uniformly positive, pointing away from the Sun. *Voyager 2* observed a transition from the unipolar region to the sector zone between  $\sim 2012.45$  and 2013.82 (Burlaga et al. 2017),

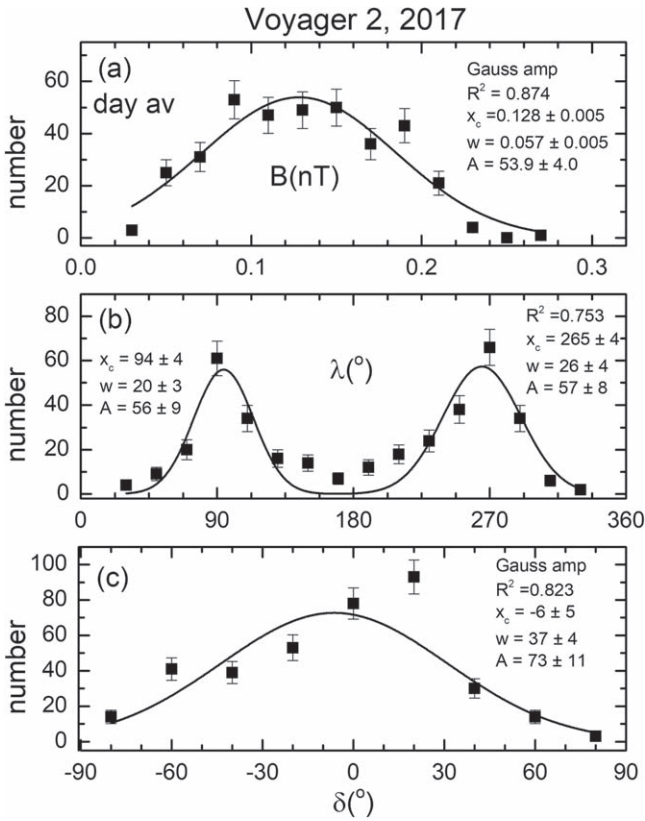


**Figure 4.** Distributions of daily averages of (a)  $B$ , (b) the azimuthal angle  $\lambda$ , and (c) the elevation angle  $\delta$ . The distribution of  $B$  is a Gaussian distribution. The azimuthal angle  $\lambda$  is described by two Gaussian distributions with two peaks of nearly equal magnitude at  $90^\circ$  and  $270^\circ$ , respectively. The distribution of  $\delta$  is approximately a Gaussian distribution centered at  $0^\circ$ .

after which it continued to observe sectors through at least 2017.

The distribution of the daily averages of  $B$  during 2017 is shown in Figure 4(a). This distribution is closely approximated (coefficient of determination  $R^2 = 0.874$ ) by a Gaussian distribution that has a maximum at  $0.128 \pm 0.005$  nT, consistent with the average magnetic field strength observed during 2017. This distribution is qualitatively different from the lognormal distribution of  $B$  observed by V2 during 2015 (Burlaga et al. 2017). The difference between the two distribution functions is largely due to the presence of a GMIR during 2015 that was observed for more than a solar rotation and contained very strong magnetic fields, up to 0.35 nT. The strong magnetic fields appeared as a tail in the lognormal distribution describing the V2 observations during 2015. GMIRs are more likely to be observed near the projected maximum of solar activity (2015) than during the projected declining phase (2017).

The distribution of azimuthal angles observed by V2 during 2017 shown in Figure 4(b) has two peaks (near the Parker spiral angles  $90^\circ$  and  $270^\circ$ ), just as V2 observed during 2015. The distribution of elevation angles observed by V2 during 2017 (Figure 4(c)) was fit reasonably well by a Gaussian distribution with a peak at  $-6^\circ \pm 5^\circ$ , consistent with  $0^\circ$ , as is generally observed in the solar wind and heliosheath. However, one should note the point at  $\delta = 20^\circ$ , which is statistically above the Gaussian curve.

Figure 5(a) shows the daily averages of the magnetic field strength as a function of time. The average magnetic field

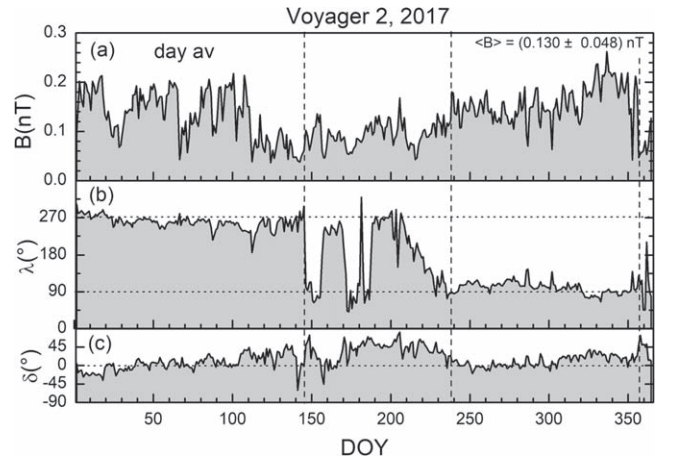


**Figure 5.** (a) Daily averages of  $B(t)$ , (b) azimuthal elevation angle  $\lambda(t)$ , and (c) elevation angle  $\delta(t)$  measured in the heliosheath by V2 during 2017. The underlying magnetic field is close to the Parker spiral magnetic field ( $\lambda = 270^\circ$  and  $90^\circ$ , and  $\delta = 0^\circ$ ) for the most part. An “away” (+) sector was observed during the beginning of the year, and a “toward” (−) polarity sector was observed during the last part of the year. At least two brief “away” polarity sectors and two brief “toward” polarity sectors were observed during the middle of the year, but these sectors were anomalous in that they were associated with large values of the elevation angle throughout most of the interval between day 146 and day 239.

strength  $\langle B \rangle = 0.13 \pm 0.05$  nT observed during 2017 is comparable to that observed near solar maximum during 2015, namely,  $\langle B \rangle = 0.13 \pm 0.05$  nT. Note that the magnetic fields near the beginning and end of 2017 were stronger than those observed during the middle of 2017 (Burlaga et al. 2018). In particular,  $B$  is relatively weak in the broad transition region between the away and toward polarities.

Figures 5(b) and (c) show that the magnetic field direction was close to the “away” Parker spiral angle  $270^\circ$  during the first 146 days of the year and was close to the “toward” Parker spiral field direction  $90^\circ$  from day 239 through day 365 (Parker 1958, 1961), indicating a change in the polarity of the magnetic field at V2 during 2017. There appear to be four small sectors between the two large sectors with opposite polarity, between day 146 and day 239. However, the elevation angles were relatively large and positive, differing significantly from the value  $\delta = 0$  for the corresponding Parker spiral angle. Note that when the elevation angle is  $90^\circ$ , the azimuthal angle is undefined.

In order to understand the transition between the extended positive- and negative-polarity regions at the beginning and end of 2017 and the narrow “sectors” in the middle of 2017 (Figure 5(b)), it is necessary to consider the components of  $B$  in a spacecraft-centered RTN coordinate system. In this coordinate system, the only nonzero component of the Parker spiral magnetic field is the  $BT$  component; the  $BN$  and  $BR$  components of the ideal Parker spiral magnetic field are equal to zero. Figure 6(d) shows that the average value of  $BR$  was  $-0.016 \pm 0.029$  nT during 2017, and Figure 6(c) gives an intermediate value for the average value of  $BN = 0.027 \pm 0.047$  nT.

Figures 6(b)–(d) shows the  $BT$ ,  $BN$ , and  $BR$  components, respectively, of the magnetic fields observed by V2 during 2017. Since the  $BT$  component is dominant, the overall sector structure is best understood by considering  $BT$  as a function of time. The  $BT$  component is positive in the direction of the motion of the planets, and the  $BR$  component is directed

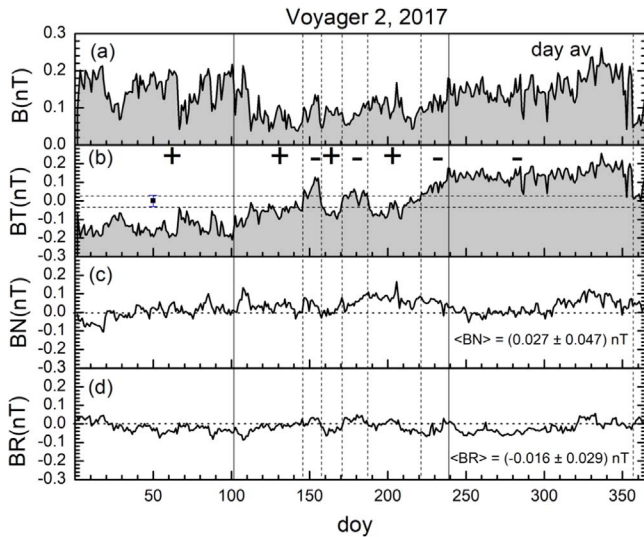


**Figure 6.** Temporal variations of daily averages of (a)  $B$ , (b) the  $BT$  component of  $B$ , (c) the  $BN$  component of  $B$ , and (d) the  $BR$  component of  $B$ , where the components refer to the spacecraft-centered RTN coordinate system. The dominant component of the magnetic field is the  $BT$  component, which shows the largest variations. However, there was an interval from day 146 to day 239 during which  $BT$  was nearly zero, with relatively small fluctuations having positive and negative polarity.

radially outward from the Sun. The values of  $BT$  were negative between the beginning of 2017 and day 101, corresponding to the magnetic fields pointing “away” from the Sun along the Parker magnetic field direction, which we denote by the plus signs in Figure 6(b). The values of  $BT$  between days 239 and 365 were positive, corresponding to magnetic fields pointing toward the Sun along the Parker spiral, which we denote by minus signs. The transition of the  $BT$  component (from a large “away” sector at the beginning of 2017 to a large “toward” sector at the end of 2017) occurred during a broad interval, from day 101 to day 239.

In addition, abrupt but small changes in magnetic polarity occurred between day 146 and day 239, when the average  $BT$  component of  $B$  was  $\langle BT \rangle = 0.002 \pm 0.123$  nT, consistent with zero within the uncertainty of the observations! The five “sectors” shown in this interval in Figure 6 were associated with small fluctuations in  $BT$ ,  $BN$ , and  $BR$ . Note that the average  $BN$  component during this interval was only  $\langle BN \rangle = 0.027 \pm 0.047$  nT, and the average  $BR$  component was even smaller,  $\langle BR \rangle = -0.016 \pm 0.029$  nT. Both  $BR$  and  $BN$  were close to the noise level of the instrument, but there were a few regions with relatively large magnitudes of  $BR$  and  $BN$ , giving apparent sectors. The uncertainties in the  $BR$  and  $BT$  components are generally close to  $\pm 0.03$  nT, as shown by the error bar in  $BT$  on day 50 in Figure 6(b).

The observations of  $BN$  in Figure 6 suggest that the HCS was very close to the latitude of V2 ( $-31.6^\circ$ ), with small ripples giving statistically significant fluctuations corresponding to the two small positive-polarity regions and the three small negative-polarity regions indicated by the plus and minus signs, respectively, between approximately day 146 and day 239 in Figure 6(b). This result is consistent with the observation that the HCS moved toward the solar ecliptic plane during the declining phase of solar cycle.

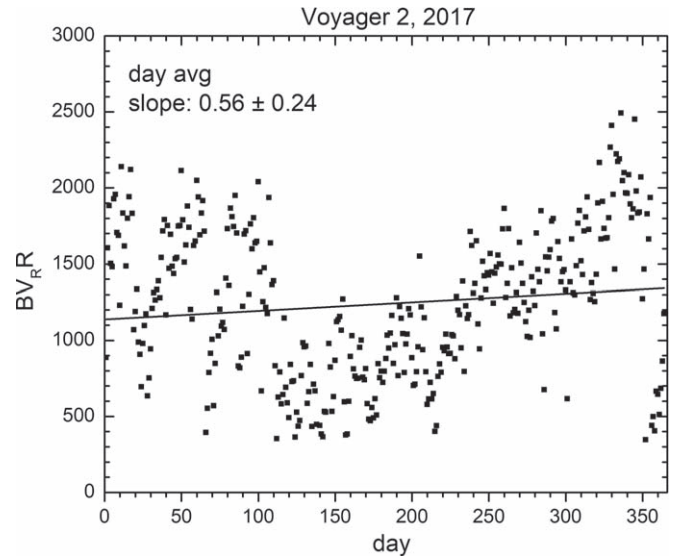


**Figure 7.** Estimate of the magnetic flux,  $BV_R R$ , as a function of time. A linear fit to the observations shows that there was no net flux deficit during 2017.

#### 4.2. Magnetic Reconnection in the Distant Heliosheath?

Parker (1958, 1961) predicted that  $BV_R R$ , where  $R$  is distance from the Sun, should be constant for a stationary radial MHD flow. A decrease in  $BV_R R$  at VI was observed by Krimigis et al. (2011), which they attributed to a decrease in  $V_R$  with time. (Although VI does not have an operating plasma instrument, approximate values of the velocity can be computed from the Low Energy Charged Particle instrument.) The velocity component  $V_R$  reached zero and even had negative values during 2011 and 2012, while  $B$  remained relatively constant. On the other hand, a number of theoretical papers suggest that magnetic reconnection can be significant in large-scale flows in the heliosheath.

Opher (2012), assuming that  $BV_R R$  remains constant, argued that the decrease of the speed to  $V_R = 0$  observed at VI implies a large increase in  $B$ , which was not observed. They proposed that the excess magnetic energy was dissipated by the process of magnetic reconnection. Using an MHD model, Provornikova et al. (2013, 2014) and Michael et al. (2015) predicted that the speed at VI should be a constant rather than decreasing before the heliopause is observed. They interpreted the decrease in magnetic flux observed by VI as a result of magnetic reconnection. Pogorelov et al. (2012b) offered a dynamical explanation for the decrease in speed and magnetic flux observed by VI, but Pogorelov et al. (2017) provided a model that does predict magnetic reconnection in the heliosheath. Pogorelov et al. (2017) show that instabilities may also occur in the heliosheath, but these do not necessarily result in a decrease in the magnetic flux.

Richardson & Burlaga (2013) showed that the predicted number of sector boundaries was equal to the number expected in the heliosheath, consistent with no magnetic reconnection, but there were a few cases in which equality was not observed, which might be interpreted as the result of magnetic reconnection. Examination of the magnetic fields and the velocity at a sector boundary observed by V2 during 2015 by Burlaga et al. (2018) showed no evidence for reconnection in a relatively thin current sheet associated with a sector boundary.

Figure 7 shows that a net increase in  $BV_R R$  was observed by V2 during 2017, rather than a decrease, which would occur if



magnetic reconnection were significant. The increase was largely the result of the overall increase in  $B$  observed by V2 during 2017. Strictly speaking, the magnetic flux is conserved only if the flow is radial and stationary, but Richardson & Decker (2014) show that the flow is diverted away from the radial direction in the outer heliosheath, and our observations show that the flow was nonstationary.

Nevertheless, there is no compelling direct evidence in V2 2017 data for significant dissipation of magnetic fields by resistivity associated with magnetic reconnection, even in the distant heliosheath. It cannot be said that magnetic reconnection does not occur based on observations alone. It might be argued that the relatively weak magnetic fields associated with the sector boundaries in the middle of 2017 were a consequence of magnetic reconnection possibly occurring prior to 2017. The possibility of reconnection in the heliosheath cannot be excluded, since it might be occurring in regions of the current sheet not sampled by the spacecraft. It is more likely that the relatively strong fields observed in the merged interaction regions were produced by the compression of relatively weak magnetic fields by the overtaking of slow flows by fast flows, which is routinely observed between 1 and 10 au (Burlaga 1995).

#### 4.3. Merged Interaction Regions and Cosmic Rays during 2017

An empirical relationship between the changes in the cosmic-ray intensity (CRI) and the magnetic field was observed in the solar wind at 11 au during 2000 (Burlaga et al. 1985), and it has been observed throughout the region beyond 11 au and into the distant heliosheath. Basically, this relationship indicates that, during a given year, the CRI decreases at a rate proportional to  $B$  when  $B$  is greater than the average value for the year, the CRI is constant when  $B$  is equal to the average value during the year, and the corresponding CRI increases at a constant rate when  $B$  is less than the average magnetic field strength. In most cases, this relationship can be described by two parameters (a recovery rate and a “diffusion” rate) and the observed initial values of  $B$  during the year. Generally, the regions with strong magnetic fields that produce the decrease in the cosmic-ray rate are associated with MIRs that extend over a limited range of latitudes, as well as the GMIRs that extend around the Sun and up to high latitudes, forming effective barriers to the entry of cosmic rays (Burlaga et al. 1993). An “interaction region” in the solar wind near 1 au is a region of enhanced total pressure (magnetic pressure plus plasma pressure; Burlaga & Ogilvie 1970; Burlaga 1995, chap. 7, p. 115).

Three merged interaction regions are shown in Figure 8(b), and the CRI is shown in Figure 8(a). When the first two MIRs moved past V2 between day 30 and day 110, the CRI decreased. When the magnetic field was weaker than the average between day 110 and day 180, the CRI increased, and when  $B$  was close to the average value between day 150 and day 210, the CRI was relatively constant. Between day 210 and day 280, the CRI increased when  $B$  was increasing from low values to values above the average. Finally, from day 283 to day 350 the CRI decreased while the magnetic field was stronger than average. Note that overall the CRI increased during 2017. In contrast, during 2015 there was a net increase in the CRI during the first part of the year, but the passage of a GMIR reduced the CRI to the initial value. Figure 8(c) shows  $NV^2$ , which is proportional to the ram pressure or momentum

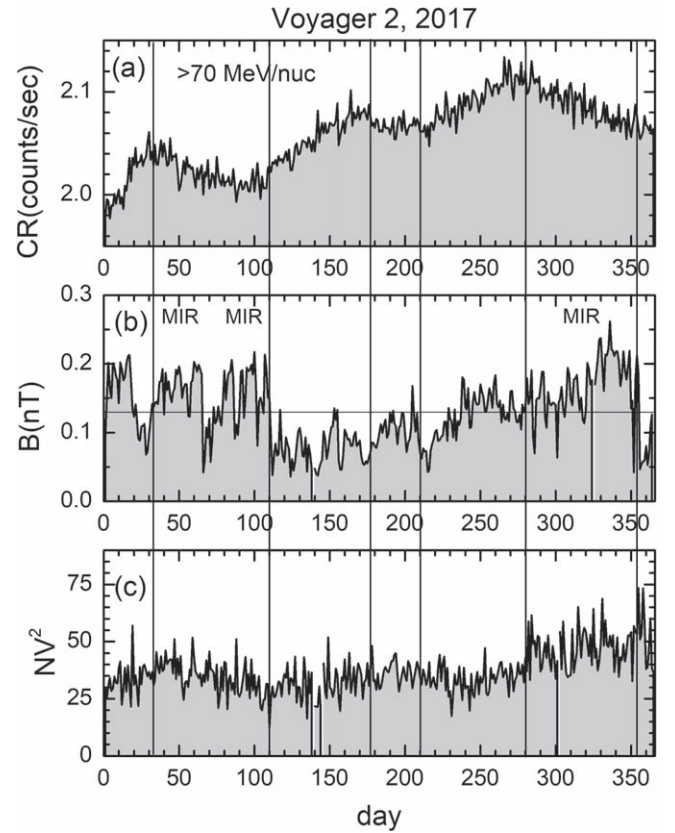


**Figure 8.** (a) Counting rate of the 70 MeV nucleon<sup>-1</sup> cosmic rays, (b) magnitude of the magnetic field, and (c)  $NV^2$  as a function of time. In most cases the CRI decreased when  $B$  was greater than average, increased when  $B$  was less than average, and remained nearly constant when  $B$  was close to the average value.

flux, as a function of time during 2017. Note that this quantity was also relatively high from day 280 to day 350, when  $B$  was large and an MIR was observed. Richardson et al. (2017) showed that GMIRs are usually (but not always) associated with large values of  $NV^2$ .

Richardson et al. (2017) showed that starting in 2012, associated with the first of the two maxima in the sunspot cycle 24, “pressure peaks” were observed by V2 in the heliosheath. The timing is consistent with the MIRs observed by V2 driving the transient disturbances in the magnetic fields of the VLISM observed by VI. The largest MIR in the heliosheath that they discussed was observed by V2 in late 2015, which is shown in Figure 11 of Burlaga et al. (2018). Richardson et al. (2017) predicted that the associated shock or disturbance should reach VI during 2018.

#### 4.4. Increments of $B$ , Intermittency, Turbulence, and Filaments

Intermittency was first observed in the magnetic field of the solar wind at 1 au by Burlaga (1991), consistent with the presence of both magnetic turbulence (Frisch 1995) and filamentary structure. Intermittency is a general feature of turbulence in fluids and appears in the multifractal structure in the solar wind (Burlaga 1995; Burlaga & Ness 2013; Bruno 2019). Throughout the heliosheath, the magnetic fluctuations on scales  $\tau$  less than several days have been found to be intermittent and filamentary. The distribution of increments of  $B$  on scale  $\tau$  ( $dB = B(t + \tau) - B(t)$ ) in the heliosheath (Burlaga et al. 2006) is generally a  $q$ -Gaussian



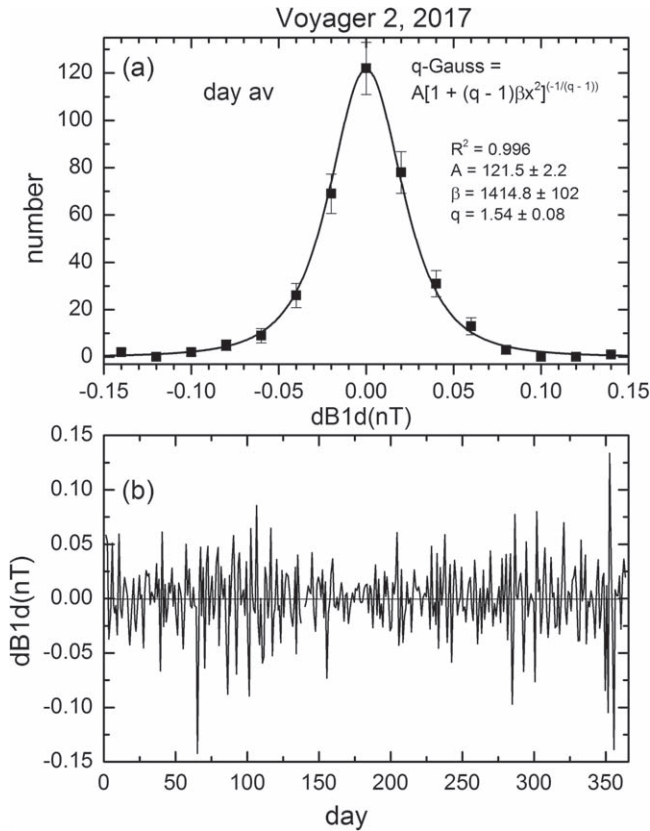


**Figure 9.** (a) Distribution of daily increments of  $B$  observed by V2 during 2017. The solid curve is a fit to the  $q$ -Gaussian distribution with the parameters shown in the figure. (b) Plot of the daily increments of  $B$  as a function of time showing the intermittent character of the fluctuations.

distribution function of nonextensive statistical mechanics (Tsallis 1988, 2004), which is proportional to  $[1 + (q-1)\beta x^2]^{-1/(q-1)}$ . This function is related to the  $\kappa$ -distribution, which is found in a great variety of thermal processes (Livadiotis 2018). In nonextensive statistical mechanics  $q$  is called the “nonextensivity index.” The  $q$ -Gaussian distribution reduces to a Gaussian distribution in the limit  $q = 1$ .

Thus, it is not surprising to find that  $q$ -Gaussian distributions of increments of  $B$  were also observed in the 2017 data from V2. On each day there were data gaps at least several hours long as, well as smaller gaps throughout the data set. Therefore, we calculated increments of  $B$  on a scale of 1 hr (described by the increments  $dB1h = B(t+1h) - B(t)$ ) and on a scale of 1 day (described by the increments  $dB1d = B(t+1d) - B(t)$ ) for successive hours and days for which we have measurements from V2. The resulting observations of the hourly and daily increments of  $B$  are shown in Figures 9(b) and 10(b), respectively. The intermittency of the fluctuations of  $dB1h(t)$  and  $dB1d(t)$  is obvious. The associated distribution functions are shown in Figures 9(a) and 10(a), respectively. These distribution functions can be described very accurately by the  $q$ -Gaussian distribution  $A_q \times [1 + (q-1)\beta x^2]^{-1/(q-1)}$ .

For the distribution of increments of hourly averages (Figure 9(a)), this function provides an excellent fit to the data ( $R^2 = 0.990$ ), giving  $A = 991 \pm 5$ ,  $\beta = 17427 \pm 41$ , and  $q = 1.64 \pm 0.02$ . Similarly, the distribution of increments of daily averages (Figure 10(a)) gives  $R^2 = 0.996$ ,  $A = 122 \pm 2$ ,  $\beta = 1415 \pm 100$ , and  $q = 1.54 \pm 0.08$ . Similar results were

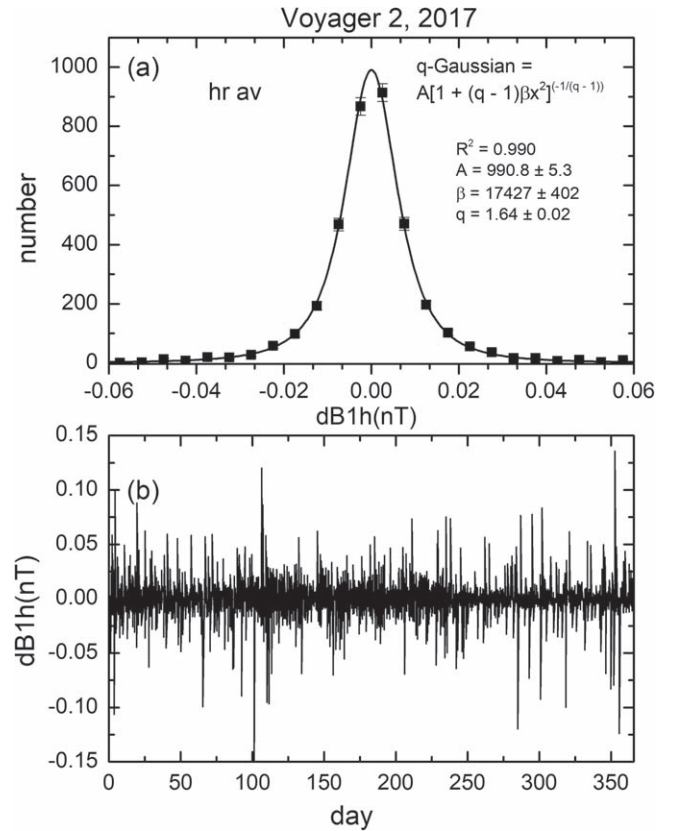


**Figure 10.** (a) Distribution of hourly increments of  $B$  observed by V2 during 2017. The solid curve is a fit to the  $q$ -Gaussian with the parameters shown in the figure. (b) Plot of the hourly increments of  $B$  as a function of time showing the intermittent character of the fluctuations.

obtained for the V2 observations made during 2015 (Burlaga et al. 2018). Thus,  $q \approx 1.6$  is a general, but not universal, property of the magnetic field observations in the distant heliosphere and heliosheath, including the very distant heliosheath.

## 5. Summary and Discussion

*Voyager 1* observed a large magnetic structure in the draped interstellar magnetic field observed upstream of the heliopause, beginning on 2016 day 341 and extending through 2017. The magnetic field strength increased in a magnetic pressure front and diminished slowly and nearly monotonically with increasing time following the pressure front throughout 2017. There was no change in the direction of the magnetic field throughout the large magnetic structure. There was one interval within the large magnetic structure that began and ended abruptly and contained quasi-periodic oscillations in  $B$  with small but statistically significant amplitudes accompanied by noise from the instrument and spacecraft. The origin and evolution of this wave and the fluctuations are not yet known.





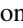
This paper also discusses the heliosheath magnetic field, cosmic rays, and plasma observed by V2 during 2017, when the spacecraft was in the distant heliosheath, approaching the heliopause. The V2 observations during 2017 were made during the declining phase of solar cycle 24. Global merged interaction regions with very strong fields were not observed, but merged interaction regions of more limited extent with magnetic field strength of the order of 0.2 nT were observed, and they might be capable of perturbing the position of the

heliopause. Further studies are needed to obtain a clear understanding of the relationships between the magnetic fields and plasmas in the heliosheath and those in the VLISM (which are influenced by magnetic field draping and the plasma flow around the heliopause).

The properties of the distant heliosheath during 2017 in the declining phase of the solar cycle 24 were similar to the properties that have been observed previously in the heliosheath. The average magnetic field strength was  $0.13 \pm 0.05$  nT. Merged interactions were present, which modulated the cosmic rays in accordance with the “CR-B relationship” that has been observed since V2 was at 10 au. An unusual transition from a positive-polarity sector and a negative-polarity sector was observed by V2 during 2017. This transition might be related to the motion of the HCS past V2 as it moved toward the solar equatorial regions during the declining phase of solar cycle 24. At smaller scales, the daily and hourly increments of  $B$  during 2017 were proportional to the  $q$ -Gaussian distribution with the value of  $q$  approximately 1.6, consistent with most earlier measurements by V1 and V2 in the heliosheath. The  $q$ -Gaussian distribution appears to be a universal property of the distant heliosphere, related to the filamentary structure of the magnetic field and compressive turbulence in the magnetic field observed over a range of scales, which is more completely described by a multifractal analysis.

J.P. was supported by an appointment to the NASA Postdoctoral Program at the NASA Goddard Space Flight Center, administered by Universities Space Research Association under contract with NASA. D.B. and N.F.N. were supported by the NASA *Voyager* Project under a cooperative agreement to the University of Maryland, Baltimore County. L. F.B. was supported by NASA contract 80GSFC19C0012. P.M. was supported by the NASA Earth and Space Science Fellowship Program-grant 16-HELIO16F-0022, and J.R. was supported by NASA under grant 959203 from the Jet Propulsion Laboratory to the Massachusetts Institute of Technology.

## ORCID iDs

L. F. Burlaga  <https://orcid.org/0000-0002-5569-1553>  
 L. K. Jian  <https://orcid.org/0000-0002-6849-5527>  
 J. Park  <https://orcid.org/0000-0002-8989-4631>  
 P. Mostafavi  <https://orcid.org/0000-0002-3808-3580>  
 J. D. Richardson  <https://orcid.org/0000-0003-4041-7540>

## References

- Baranov, V. B., & Ruderman, M. S. 2013, *MNRAS*, **434**, 3202  
 Baranov, V. B., & Zaitsev, N. A. 1998, *GeoRL*, **25**, 4051  
 Borovikov, S. N., Pogorelov, N. V., & Ebert, R. W. 2012, *ApJ*, **750**, 42  
 Bruno, R. 2019, *E&SS*, in press  
 Burlaga, L. 1991, *JGR*, **640**, 5847  
 Burlaga, L. 1995, *Interplanetary Magnetohydrodynamics* (New York: Oxford Univ. Press)  
 Burlaga, L., Ness, N. F., Acuña, M. H., et al. 2008, *Natur*, **454**, 75  
 Burlaga, L. F., McDonald, F., Goldstein, M. L., & Lazarus, A. J. 1985, *JGR*, **90**, 12027  
 Burlaga, L. F., & Ness, N. F. 2013, *ApJ*, **765**, 35  
 Burlaga, L. F., & Ness, N. F. 2016, *ApJ*, **829**, 134  
 Burlaga, L. F., Ness, N. F., & Richardson, J. D. 2014, *JGR*, **119**, 6062  
 Burlaga, L. F., Ness, N. F., & Richardson, J. D. 2017, *ApJ*, **841**, 47  
 Burlaga, L. F., Ness, N. F., & Richardson, J. D. 2018, *ApJ*, **861**, 9  
 Burlaga, L. F., Ness, N. F., Stone, E., & McDonald, F. B. 2011, *JGR*, **116**, A12104  
 Burlaga, L. F., Ness, N. F., & Stone, E. C. 2013, *Sci*, **341**, 147  
 Burlaga, L. F., & Ogilvie, K. W. 1970, *SoPh*, **15**, 61  
 Burlaga, L. F., Perko, J., & Pirraglia, J. 1993, *ApJ*, **407**, 347  
 Burlaga, L. F., Viñas, A. F., Ness, N. F., & Acuña, M. H. 2006, *ApJL*, **644**, L83  
 Decker, R. B., Krimigis, S. M., Roelof, E. C., et al. 2008, *Natur*, **454**, 67  
 Fermo, R. L., Pogorelov, N. V., & Burlaga, L. F. 2015, *J. Phys. Conf. Ser.*, **642**, 012008  
 Fisk, L. A., & Gloeckler, G. 2014, *JGR*, **119**, 8733  
 Frisch, U. 1995, *Turbulence: The Legacy of A.N. Kolmogorov* (Cambridge: Cambridge Univ. Press)  
 Gloeckler, G., & Fisk, L. 2016, *ApJ*, **833**, 290  
 Gurnett, D. A., & Kurth, W. S. 2008, *Natur*, **454**, 78  
 Gurnett, D. A., Kurth, W. S., Allendorf, S. C., & Poynter, R. L. 1993, *Sci*, **262**, 199  
 Gurnett, D. A., Kurth, W. S., Burlaga, L. F., & Ness, N. F. 2013, *Sci*, **341**, 1489  
 Gurnett, D. A., Kurth, W. S., Stone, E. C., et al. 2015, *ApJ*, **809**, 121  
 Gurnett, D. A., Kurth, W. S., Stone, E. C., et al. 2018, *AGUFM*, SH21B-03  
 Holzer, T. E. 1989, *ARA&A*, **27**, 99  
 Jian, L. K., Russell, C. T., & Luhmann, J. G. 2011, *SoPh*, **274**, 321  
 Kim, T. K., Pogorelov, N. V., & Burlaga, L. F. 2017, *ApJL*, **843**, 32  
 Krimigis, S. M., Decker, R. B., Roelof, E. C., et al. 2013, *Sci*, **341**, 144  
 Krimigis, S. M., Roelof, E. C., Decker, R. B., & Hill, M. E. 2011, *Natur*, **474**, 359  
 Liu, Y., Richardson, J. D., Belcher, J. W., & Kasper, J. C. 2007, *ApJL*, **659**, L65  
 Liu, Y. T., Richardson, J. D., Wang, C., & Luhmann, J. G. 2014, *ApJL*, **788**, L28  
 Livadiotis, G. 2018, *EL*, **122**, 50001  
 McComas, D. J., Dayeh, M. A., Funsten, H. O., et al. 2018, *ApJL*, **856**, 10  
 Michael, M., Opher, E., Provornikova, E., Richardson, J., & Toth, G. 2015, *ApJL*, **803**, L6  
 Mostafavi, P., & Zank, G. P. 2018a, *ApJL*, **854**, L15  
 Mostafavi, P., & Zank, G. P. 2018b, *J. Phys. Conf. Ser.*, **1100**, 012018  
 Opher, M. 2012, *AstRv*, **7**, 68  
 Opher, M., Drake, J. F., Swisdak, M., et al. 2011, *ApJ*, **734**, 71  
 Parker, E. N. 1958, *ApJ*, **128**, 664  
 Parker, E. N. 1961, *ApJ*, **134**, 20  
 Pogorelov, N., Borovikov, S., Heerikhuisen, J., et al. 2014, in Proc. 2014 Annual Conf. Extreme Science and Engineering Discovery Environment, ed. S. Lathrop & J. Alameda (Alameda, NY: ACM), 22  
 Pogorelov, N. V., Borovikov, S. N., Burlaga, L. F., et al. 2012a, in AIP Conf. Ser. 1436, *Physics of the Heliosphere: A 10-year Retrospective*, ed. J. Heerikhuisen et al. (Melville, NY: AIP), 321  
 Pogorelov, N. V., Borovikov, S. N., Zank, G. P., et al. 2012b, *ApJL*, **750**, L4  
 Pogorelov, N. V., Heerikhuisen, J., Roytershteyn, V., et al. 2017, *ApJ*, **245**, 9  
 Pogorelov, N. V., Suess, S. T., Borovikov, S. N., et al. 2013, *ApJ*, **772**, 2  
 Provornikova, E., Opher, E. M., Izmodenov, V. V., Richardson, J. D., & Toth, G. 2014, *ApJ*, **794**, 29  
 Provornikova, E., Opher, M., Izmodenov, V., & Toth, G. 2013, *A&A*, **552**, A99  
 Richardson, J. D. 2017, *J. Phys. Conf. Ser.*, **900**, 012017  
 Richardson, J. D., & Burlaga, L. F. 2013, *SSRv*, **176**, 217  
 Richardson, J. D., & Decker, R. B. 2014, *ApJ*, **792**, 126  
 Richardson, J. D., Kasper, J. C., Wang, C., Belcher, J. W., & Lazarus, A. J. 2008, *Natur*, **454**, 63  
 Richardson, J. D., Wang, C., Liu, Y. D., et al. 2017, *ApJ*, **834**, 190  
 Stone, E. C., Cummings, A. C., McDonald, F. B., et al. 2008, *Natur*, **454**, 71  
 Stone, E. C., Cummings, A. C., McDonald, F. B., et al. 2013, *Sci*, **341**, 150  
 Tsallis, C. 1988, *JSP*, **52**, 479  
 Tsallis, C. 2004, in *Nonextensive Entropy: Interdisciplinary Applications*, ed. M. Gell-Mann & C. Tsallis (New York: Oxford Univ. Press), 1  
 Washimi, H., Tanaka, T., & Zank, G. P. 2017, *ApJL*, **846**, L9  
 Washimi, H., Zank, G. P., Hu, Q., et al. 2011, *MNRAS*, **416**, 147  
 Whang, Y. C. 2010, *ApJ*, **710**, 936  
 Whang, Y. C., & Burlaga, L. F. 1995, *JGR*, **100**, 17023  
 Zank, G. P. 2015, *ARA&A*, **53**, 449  
 Zank, G. P., & Müller, H.-R. 2003, *JGRA*, **108**, 1240  
 Zank, G. P., Pauls, H. L., Williams, L. L., & Hall, D. T. 1996, *JGR*, **101**, 21639  
 Zirnstein, E. J., Heerikhuisen, J., Funsten, H. O., et al. 2016, *ApJL*, **818**, L18  
 Zirnstein, E. J., Heerikhuisen, J., McComas, D. J., et al. 2018, *ApJ*, **859**, 104